Applied Physics Letters ARTICLE pubs.aip.org/aip/apl

Shubnikov–de Haas oscillations of 2DEGs in coherently strained AlN/GaN/AlN heterostructures on bulk AlN substrates

Cite as: Appl. Phys. Lett. **126**, 202101 (2025); doi: 10.1063/5.0264000
Submitted: 7 February 2025 · Accepted: 30 April 2025 ·
Published Online: 19 May 2025

View Online Export Citation CrossMark

Yu-Hsin Chen,[1,a] Jimy Encomendero,[2] Chuan F. C. Chang,[3] Huili Grace Xing,[1,2,4] and Debdeep Jena[1,2,4,b]

AFFILIATIONS

[1]Department of Materials Science and Engineering, Cornell University, Ithaca, New York 14853, USA
[2]School of Electrical and Computer Engineering, Cornell University, Ithaca, New York 14853, USA
[3]Department of Physics, Cornell University, Ithaca, New York 14853, USA
[4]Kavli Institute at Cornell for Nanoscale Science, Cornell University, Ithaca, New York 14853, USA

[a]Author to whom correspondence should be addressed: yc794@cornell.edu
[b]Electronic mail: djena@cornell.edu

ABSTRACT

We report the observation of Shubnikov–de Haas (SdH) oscillations of two-dimensional electron gases (2DEGs) in coherently strained, low-dislocation undoped and δ-doped AlN/GaN/AlN heterostructures on bulk AlN. The oscillations reveal a single subband occupation in the undoped and two subband occupation in the δ-doped sample. More importantly, SdH oscillations enable direct measurement of critical 2DEG parameters at the Fermi level: carrier density and ground state energy level, electron effective mass ($m^* \approx 0.289\, m_e$ for undoped and $m^* \approx 0.298\, m_e$ for δ-doped sample), and quantum scattering time ($\tau_q \approx 83.4$ fs for undoped and $\tau_q \approx 130.6$ fs for δ-doped sample). These findings provide important insights into the fundamental properties of 2DEGs that are quantum confined in the thin GaN layers, essential for designing nitride heterostructures for high-performance electronic applications.

The discovery of polarization-induced two-dimensional electron gases (2DEGs) in AlGaN/GaN heterojunctions in the 1990s revolutionized the development of high-electron mobility transistors (HEMTs).[1,2] These GaN-based devices, characterized by their wide bandgaps, high electron velocities, and ability to form heterojunctions with high carrier concentration and mobility, have since become essential for high-frequency RF amplifiers[3,4] and fast high-voltage switching applications.[5,6]

More recently, 2DEGs have been demonstrated in a thin, coherently strained GaN well sandwiched between AlN buffer and AlN top barrier.[7–10] These AlN/GaN/AlN heterostructures, epitaxially grown on single-crystal AlN substrates, achieve a five-order reduction in dislocation density (DD) down to $\approx 10^4$ cm^{-2}.[11] While the AlN layers are strain-free due to lattice-matching with the AlN substrate, the thin GaN channel is under a large compressive strain of -2.4%, which alters its electronic band structure. The large discontinuity in spontaneous and piezoelectric polarization between GaN and AlN induces a high-density 2DEG, and the large energy band offset confines the 2DEG within the GaN channel. As a result, AlN/GaN/AlN heterostructures can achieve 2DEG densities of $n_s \sim 2$–3×10^{13} cm^{-2}, enabling access to a larger k-space in the GaN conduction band. In comparison, AlGaN/GaN heterostructures—where Shubnikov–de Haas (SdH) oscillations have been reported—exhibit lower 2DEG densities, ranging from $\sim 1 \times 10^{12}$ cm^{-2} for low Al content to $\sim 1 \times 10^{13}$ cm^{-2} for Al compositions between 20% and 30%.[12–18] Only a few studies demonstrated SdH oscillations in AlN/GaN heterostructures at higher 2DEG densities approaching $\sim 3 \times 10^{13}$ cm^{-2}.[19]

The electron mobility of 2DEGs in AlN/GaN/AlN heterostructures on bulk AlN substrates has been limited to lower values compared to AlGaN/GaN heterostructures on GaN substrates or templates, primarily due to two reasons: (1) a strong internal electric field that enhances roughness scattering,[20,21] and (2) parallel conduction due to the formation of a parallel two-dimensional hole gas (2DHG) at the opposite interface from the 2DEG. Recently, using δ-doping, the 2DHG was suppressed, and the internal electric field was reduced, resulting in improved electron mobility.[10] Here, we present a magnetotransport study of 2DEGs in such undoped and δ-doped AlN/GaN/AlN heterostructures.

A key characteristic of high-quality 2DEGs is the occurrence of quantum oscillations in longitudinal magnetoresistance R_{xx}, known as SdH oscillations. For these quantization effects to manifest in a magnetic field, the cyclotron energy $\hbar\omega_c$ must exceed both the thermal energy $k_b T$ and the Landau level broadening $\hbar/\tau_q$,[22] where $\omega_c = eB/m^*$ is the cyclotron frequency, k_b is the Boltzmann constant, τ_q is the quantum scattering time, and m^* is the electron effective mass. This condition indicates that observing quantum oscillations necessitates the application of a strong magnetic field, and the use of high-quality samples with minimal scattering. In our study, we observed well-resolved SdH oscillations in R_{xx} for both structures. These quantum oscillations allow us to extract critical parameters for 2D carrier transport, including (1) the carrier density and ground state energy levels, (2) the electron effective mass, and (3) the quantum scattering time.

Figures 1(a) and 1(c) present schematic cross sections of the undoped and δ-doped AlN/GaN/AlN heterostructures used in this study. Both samples were grown epitaxially on single-crystal AlN substrates using molecular beam epitaxy. Each sample consists of a 20 nm GaN well sandwiched between a 6 nm AlN barrier and a 500 nm AlN buffer layer, with a 1 nm GaN cap deposited on the top to prevent oxidation of the underlying AlN. In the δ-doped sample, a sheet of silicon donors with a doping density of $\sigma_\delta = 5 \times 10^{13}\ \mathrm{cm}^{-2}$ is introduced at the bottom GaN/AlN interface. The coherently strained GaN on AlN in both samples was confirmed by x-ray reciprocal space mapping, as presented in our recent publication, which also describes the growth procedure and the structural and transport characteristics of the same samples used in this magnetotransport study.[10] Low-field Hall-effect measurements show that the undoped sample exhibits a 2DEG density of $2.04 \times 10^{13}\ \mathrm{cm}^{-2}$ with electron mobility of $611.1\ \mathrm{cm}^2/\mathrm{V\,s}$ at room temperature (RT) and $1210.4\ \mathrm{cm}^2/\mathrm{V\,s}$ at 2 K. In contrast, the δ-doped sample shows a higher 2DEG density of $3.24 \times 10^{13}\ \mathrm{cm}^{-2}$ with enhanced mobilities of $854.6\ \mathrm{cm}^2/\mathrm{V\,s}$ at RT and $2234.6\ \mathrm{cm}^2/\mathrm{V\,s}$ at 2 K. Both samples exhibit a temperature-independent 2DEG density down to cryogenic temperatures, confirming their polarization-induced nature. Through capacitance–voltage measurements, we confirmed the presence of a 2DHG at the bottom GaN/AlN interface in the undoped sample. In contrast, we observed no evidence of parallel conduction in the δ-doped sample, demonstrating the effectiveness of δ-doping in suppressing unintended channels.

Magnetotransport measurements were performed on both heterostructures using indium-soldered ohmic contacts formed in a Van der Pauw configuration. The samples were placed in a physical property measurement system (PPMS) from Quantum Design with a DC excitation current of 100 μA. Although the indium contacts accessed both the 2DEG and 2DHG, SdH oscillations were not observed for 2DHG in the undoped sample—up to a magnetic field of 14 T—due to its lower mobility. Figures 1(b) and 1(d) show the R_{xx} of 2DEG as a function of the magnetic field B applied perpendicular to the sample surface, measured over the range of 9–14 T and at temperatures from 2 to 11 K. As the magnetic field increases, the amplitude of the oscillations grows due to the larger separation between Landau levels and the increased number of states within each level, causing greater fluctuations in the density of states. In contrast, the weakening of the oscillation amplitude with increasing temperature is attributed to the smearing of the Fermi–Dirac distribution near the Fermi level.[23] The onsets of the SdH oscillations were recorded at around 8 T for both samples, as shown in Fig. S1 in the supplementary material, significantly lower than similar AlN/GaN/AlN heterostructures grown on SiC substrates, where over 25 T is required to resolve quantum oscillations.[8]

To isolate the oscillatory component ΔR_{xx}, the background resistance was subtracted from the measured R_{xx}. This background is determined by averaging polynomial fits applied separately to the peaks and valleys of the SdH oscillations,[24] as shown in Fig. S2 of the supplementary material. Figures 2(a) and 2(b) show the resulting ΔR_{xx} as a function of $1/B$ for both samples, highlighting the periodic nature of the SdH oscillations in $1/B$. The oscillatory component ΔR_{xx} is given by[25–28]

$$\Delta R_{xx} \propto \frac{\chi}{\sinh(\chi)} e^{-\frac{\pi}{\omega_c \tau_q}} \cos\left(\frac{2\pi E_F}{\hbar\omega_c}\right), \tag{1}$$

where $\chi = 2\pi^2 k_B T/(\hbar\omega_c)$ and $E_F = n_s \pi\hbar^2/m^*$ is the Fermi level of 2DEG for a particular subband. The period of the oscillation $\Delta(1/B)$ is

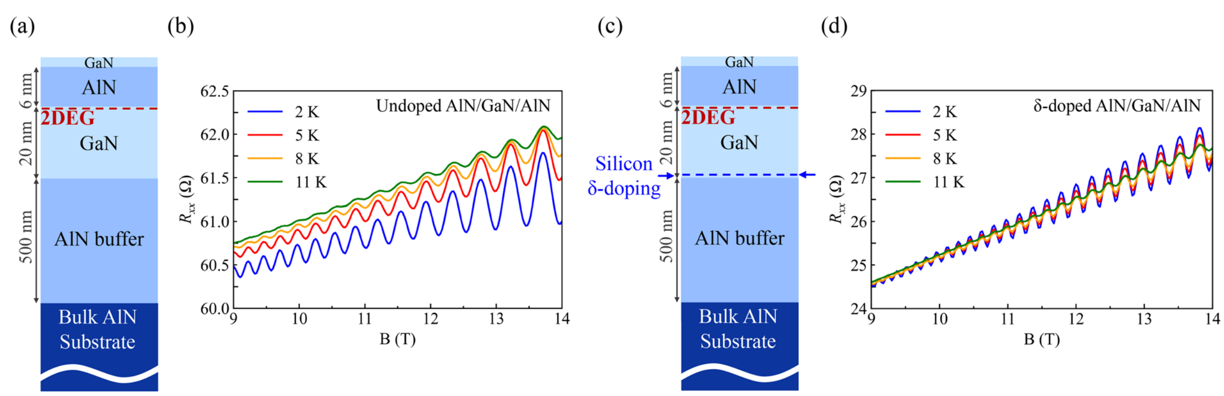

FIG. 1. (a) Schematic of the epitaxial undoped AlN/GaN/AlN heterostructure. (b) Measured longitudinal magnetoresistance R_{xx} of 2DEG in the undoped sample as a function of magnetic field B from 9 to 14 T, at various temperatures ranging from 2 to 11 K. (c) Schematic of the δ-doped AlN/GaN/AlN, which includes a sheet of silicon donors with a doping density of $\sigma_\delta = 5 \times 10^{13}\ \mathrm{cm}^{-2}$ at the bottom GaN/AlN interface, approximately 26 nm below the surface. (d) Measured R_{xx} of 2DEG in the δ-doped sample within the same magnetic field and temperature range, showing more frequent oscillations.

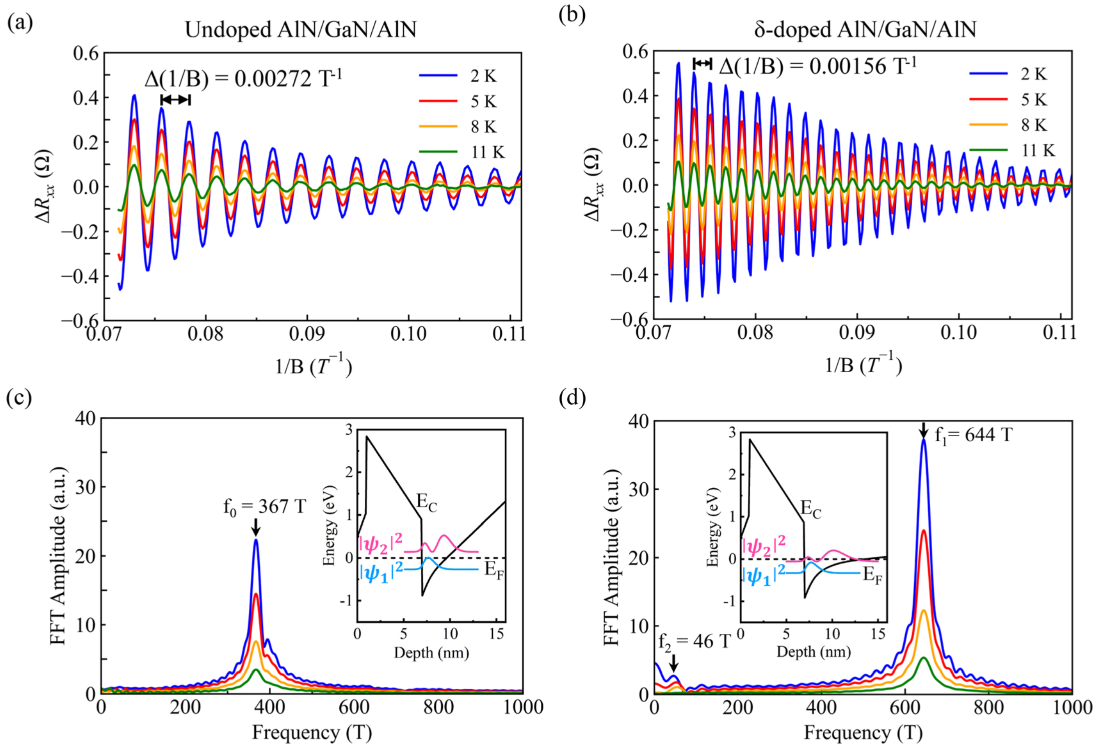

FIG. 2. (a) The oscillatory component ΔR_{xx} of the undoped sample plotted against $1/B$. The oscillations are periodic in $\Delta(1/B) = 0.002\,72\,\mathrm{T}^{-1}$, corresponding to a 2DEG density of $n_s = 1.78 \times 10^{13}\,\mathrm{cm}^{-2}$. (b) ΔR_{xx} of the δ-doped sample is periodic in $\Delta(1/B) = 0.001\,56\ \mathrm{T}^{-1}$, corresponding to a 2DEG density of $n_s = 3.11 \times 10^{13}\,\mathrm{cm}^{-2}$. (c) The fast Fourier transform (FFT) spectrum of the oscillating ΔR_{xx} vs 1/B in the undoped sample shows a single frequency at $f_0 = 367\,\mathrm{T}$, indicating single subband occupation. (d) The FFT spectrum for the δ-doped sample reveals two distinct frequency peaks at $f_1 = 644\,\mathrm{T}$ and $f_2 = 46\,\mathrm{T}$, indicating two subband occupation. The insets in (c) and (d) are the calculated conduction band energy profiles and the squared-amplitude of the electron wavefunctions for both structures, respectively.

determined by the cosine term in Eq. (1) and directly measures the 2DEG density n_s via the relation $n_s = q/(\Delta(1/B)\pi\hbar)$. For the undoped sample shown in Fig. 2(a), the oscillation periodicity is extracted as $\Delta(1/B) = 0.002\,72\,\mathrm{T}^{-1}$, corresponding to a 2DEG density of $n_s = 1.78 \times 10^{13}\,\mathrm{cm}^{-2}$. For the δ-doped sample presented in Fig. 2(b), one can observe that a higher frequency oscillation is superimposed on a lower frequency oscillation. The high-frequency oscillation, with $\Delta(1/B) = 0.001\,56\ \mathrm{T}^{-1}$, is associated with electrons occupying the first subband with $n_s = 3.11 \times 10^{13}\,\mathrm{cm}^{-2}$. The low-frequency oscillation is attributed to electrons in the second subband, which requires further analysis using fast Fourier transform (FFT) to extract its 2DEG density. The 2DEG densities extracted from $\Delta(1/B)$ exhibit an error margin of 5%.

Figures 2(c) and 2(d) present the FFT analysis of ΔR_{xx} vs $1/B$ for both samples, considering the field interval from 9 to 14 T. The insets in Fig. 2 show the calculated conduction band energy profiles and the squared-amplitude of the electron wavefunctions for both structures, obtained using a self-consistent Schrödinger–Poisson solver. These calculations indicate that the undoped sample hosts electrons in a single subband, whereas the δ-doped sample has two populated subbands. The occupation of the second subband is attributed to δ-doping, which in addition to providing more 2DEG electrons, compensates the 2DHG at the bottom interface and reduces the internal electric field in the GaN channel. This reduction in electric field lowers the confinement potential, causing the energy separation between subbands to decrease. As a result, the second subband falls below the Fermi level and becomes occupied, leading to the population of both the first and second subbands in the δ-doped sample.

From the FFT spectrum in Fig. 2(c), a single oscillation frequency at $f_0 = 367\,\mathrm{T}$ is identified for the undoped sample, confirming single subband occupation. The FFT frequency directly measures the 2DEG density, which is given by the Onsager relation: $n_s = (2q/h) \times f$, yielding $n_s = 1.77 \times 10^{13}\,\mathrm{cm}^{-2}$. This result agrees well with the electron density obtained both from the real space analysis and low-field Hall-effect measurement. In contrast to the undoped structure, the δ-doped sample shows two distinct frequency peaks in the FFT spectrum, indicating the presence of two occupied subbands [see Fig. 2(d)]. The peak at $f_1 = 644\,\mathrm{T}$ corresponds to the first subband with $n_{s1} = 3.11 \times 10^{13}\,\mathrm{cm}^{-2}$, matching the density extracted from $\Delta(1/B)$. The second peak at $f_2 = 46\,\mathrm{T}$ corresponds to electrons in the second subband with $n_{s2} = 2.22 \times 10^{12}\,\mathrm{cm}^{-2}$. The total 2DEG density $n_s = n_{s1} + n_{s2} = 3.33 \times 10^{13}\,\mathrm{cm}^{-2}$ agrees well with both the low-field Hall-effect measurement and self-consistent Schrödinger–Poisson calculations.

The Landau quantization of a 2D electron system is only due to the component of the magnetic field perpendicular to the 2D plane, $B_\perp$. By rotating the angle θ between the B field vector and the 2D plane, the period of oscillation changes according to $B_\perp = |B| \cos\theta$.

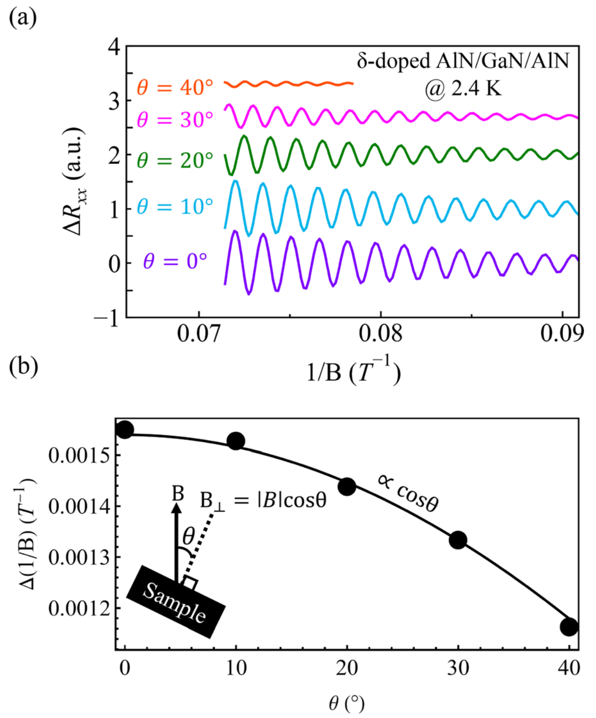

FIG. 3. (a) SdH oscillations measured at various tilt angles for the δ-doped sample at 2.4 K. The angle θ represents the tilt of the sample surface normal relative to the applied magnetic field direction, as shown in the inset of Fig. 2(b). (b) The dependence of the oscillation period $\Delta(1/B)$ on $\cos\theta$ confirms the two-dimensional confinement of electrons in the δ-doped sample.

Figure 3(a) presents the angular dependence of the SdH oscillations measured in the δ-doped sample at 2.4 K. This measurement involved rotating the normal of the 2D plane by an angle θ away from the direction of the applied B field, as depicted in the inset of Fig. 3(b). Figure 3(b) shows that the oscillation period $\Delta(1/B)$ exhibits a cosine dependence on the rotation angle θ, indicating that the oscillations solely arise from the perpendicular component of the applied magnetic field $B_{\perp}$. This characteristic behavior confirms, experimentally, the two-dimensional nature of the electron gas in the δ-doped AlN/GaN/AlN.

By analyzing the temperature-dependent SdH oscillation at a fixed B field, the effective mass of the 2DEG at the Fermi level can be determined. To achieve this, R_{xx} was measured at four different temperatures ranging from 2 to 11 K. Figure 4(a) shows the temperature dependent ΔR_{xx} for the undoped sample at various B fields. For each B field, the measured ΔR_{xx} peak values are overlaid with the best fit to the thermal damping term $\chi/\sinh(\chi)$ from Eq. (1). Numerical fitting yields an electron effective mass of $m^* = (0.289 \pm 0.003)\, m_e$ for the undoped sample, where m_e is the free electron mass. The reported electron effective mass and its error represent the mean and standard deviation of the numerically fitted values obtained across different magnetic fields. A similar analysis was done for the δ-doped sample. However, owing to its double subband occupation, a clear beating pattern is discernible in ΔR_{xx} [see Fig. 2(b)]. This beating arises from the superposition of two oscillatory components corresponding to each electronic subband. To deconvolve each oscillatory component, an inverse FFT algorithm was applied to the individual peak of the FFT spectrum. This procedure is illustrated in detail in Fig. S3 of the supplementary material. After isolating ΔR_{xx} for the first subband, its temperature dependence was analyzed to extract the electron effective mass. Numerical fitting yields $m^* = (0.298 \pm 0.001)\, m_e$ for the first subband of the δ-doped sample, as shown in Fig. 4(b). In contrast, the oscillatory component corresponding to the second subband is too weak for reliable mass extraction. The slightly higher effective mass (3.1% increase) in the δ-doped sample, compared to the undoped sample, is attributed to its higher 2DEG density. The higher 2DEG density shifts the Fermi level further away from the conduction band edge, enhancing the non-parabolicity of the conduction band and resulting in a larger effective mass. To improve the precision of electron effective mass extraction in AlN/GaN/AlN, future work will prioritize measurements at higher magnetic fields and across a broader temperature range.

The extracted electron effective masses in AlN/GaN/AlN are slightly higher than the typical value of $m^* \approx 0.2 - 0.23\, m_e$ measured in conventional AlGaN/GaN heterostructures,[12,15–18] where the GaN layer is relaxed and the 2DEG densities are lower. Several factors could contribute to these higher effective masses, including (1) the compressive strain experienced by GaN on AlN, which increases the in-plane

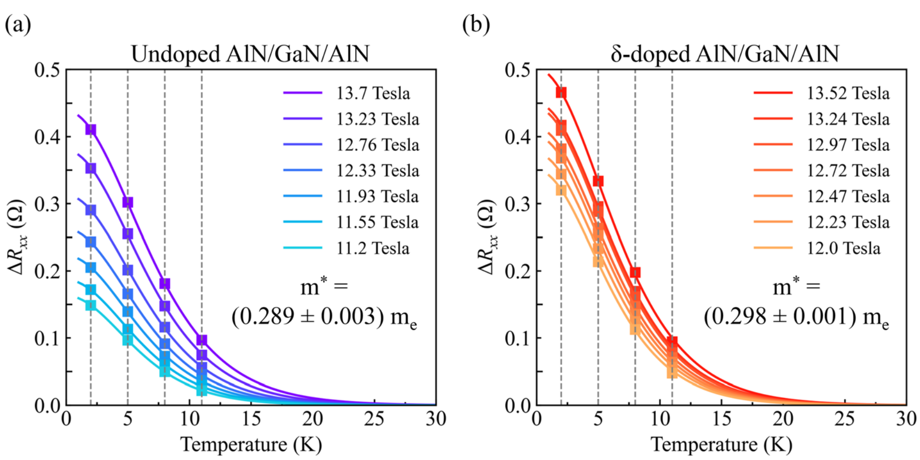

FIG. 4. Temperature dependence of ΔR_{xx} at various B fields for (a) undoped sample and (b) the first subband of δ-doped sample. Each solid curve represents the fits to $\chi/\sinh(\chi)$ in Eq. (1) at a certain B field to extract the electron effective mass. Curve fittings of the thermal damping ΔR_{xx} yield an electron effective mass of $m^* = (0.289 \pm 0.003)\, m_e$ for the undoped sample and $m^* = (0.298 \pm 0.001)\, m_e$ for the first subband of δ-doped sample. The reported electron effective mass and its error represent the mean and standard deviation of the numerically fitted values obtained across different magnetic fields.

effective mass;[29] (2) the high 2DEG densities, which push the Fermi energy further away from the subband minimum, thereby amplifying non-parabolicity effect;[30] and (3) quantum confinement, which could also play a role in enhancing the effective mass.[13] A detailed theoretical study to fully understand the effective mass of 2DEG in AlN/GaN/AlN remains an important area for future work.

The experimental measurement of both the electron effective mass m^* and the 2DEG density n_{si} for each subband allows us to accurately determine the electronic spectrum in each heterostructure. To do so, the subband population can be expressed as $n_{si} = g_{2D}(E_F - E_i)$, where E_F is the Fermi energy, E_i is the subband energy, and g_{2D} is the two-dimensional density of states, given by $g_{2D} = m^*/\pi\hbar^2$. From this analysis, we obtain that $E_F - E_1 \approx 145$ meV for the undoped sample, and $E_F - E_1 \approx 248$ meV for the δ-doped sample. The lower subband energy in the δ-doped sample results from a reduced internal electric field in the well, achieved by incorporating δ-doping. Additionally, the intersubband transition energy in the δ-doped sample is $E_2 - E_1 \approx 230$ meV, indicating that the second subband is relatively shallow (only 18 meV below E_F), with most electrons residing in the first subband.

Owing to the presence of disorder, Landau levels exhibit a finite broadening due to their coupling with various scattering potentials. This broadening can be experimentally quantified by the quantum scattering lifetime τ_q, which represents the mean time that electrons remain in one quantized orbit before scattering into another. Experimentally, τ_q determines the exponential increase in the ΔR_{xx} amplitude, as the reciprocal of the magnetic field (1/B) decreases [see Figs. 2(a) and 2(b)]. At a given temperature, τ_q is determined from the Dingle plot, where $\ln(A^*\sinh(\chi)/\chi)$ is plotted against $1/B$ and A^* represents the peak values of ΔR_{xx} (see Fig. 5). τ_q is then obtained by

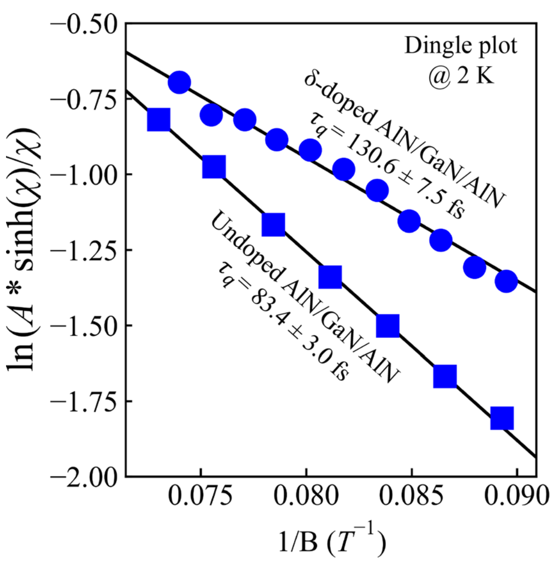

FIG. 5. The quantum scattering time τ_q is extracted from the damping of the oscillation amplitudes as a function of $1/B$. Shown here is the Dingle plot, where $\ln(A^*\sinh(\chi)/\chi)$ is plotted against $1/B$ at 2 K for the first subband of δ-doped (blue circle) and undoped (blue square) samples. A^* is the peak values of ΔR_{xx}. The solid black lines are fits to the disorder damping term $e^{-\pi/(\omega_c\tau_q)}$ from Eq. (1), yielding $\tau_q = 130.6 \pm 7.5$ fs for the first subband of δ-doped sample and $\tau_q = 83.4 \pm 3.0$ fs for the undoped sample.

fitting the data points vs $1/B$, using the disorder damping term $e^{-\pi/(\omega_c\tau_q)}$ from Eq. (1). As shown in Fig. 5, τ_q of the undoped sample is determined to be $\tau_q = 83.4 \pm 3.0$ fs at 2 K. For the δ-doped sample, precise determination of A^* was attained by isolating ΔR_{xx} of the first subband, as previously described and shown in Fig. S3. Using this approach, the quantum lifetime $\tau_q = 130.6 \pm 7.5$ fs was extracted for the first subband of the δ-doped sample.

The quantum scattering lifetime τ_q accounts for all the scattering mechanisms equally, in contrast, the momentum scattering time τ_m favors large-angle scattering over small angle scattering due to the weighting factor of $(1 - \cos\theta)$, where θ is the scattering angle.[31] Experimentally, τ_m is determined from the low-field Hall mobility via the Drude relation $\mu = e\tau_m/m^*$. At 2 K, Hall-effect mobility measurements yield $\tau_m = 198.9$ fs for the undoped sample and $\tau_m = 378.6$ fs for the δ-doped sample. The Dingle ratios $\tau_m/\tau_q \sim 2 - 3$, being close to unity for both samples, suggest the prevalence of short-range isotropic scattering potentials, likely due to temperature-independent IR scattering,[31,32] which was previously identified as the primary scattering mechanism at cryogenic temperatures for both AlN/GaN/AlN heterostructures.[10]

The electron effective mass and quantum lifetime can also be extracted by directly calculating the SdH oscillations and identifying the combination of m^* and τ_q that minimizes the root mean square (RMS) error relative to the measured ΔR_{xx} oscillations. This method was applied to the undoped sample, yielding the lowest RMS when $m^* = 0.292\, m_e$ and $\tau_q = 84$ fs, which closely matches the values extracted from fitting the thermal damping ΔR_{xx} and the Dingle plot.

In summary, 2DEGs in coherently strained undoped and δ-doped AlN/GaN/AlN heterostructures, grown on low-dislocation density single-crystal AlN substrates, exhibit SdH oscillations. FFT analysis of SdH oscillations confirms a single subband occupation in the undoped sample and double subband occupation in the δ-doped sample. Analysis of their thermal damping allows us to directly measure electron effective mass, yielding $m^* \approx 0.289\, m_e$ for the undoped sample and $m^* \approx 0.298\, m_e$ for the δ-doped sample, highlighting a fundamental distinction compared to AlGaN/GaN heterostructures with $m^* \approx 0.2 - 0.23\, m_e$. Furthermore, analysis of the Dingle plot reveals a longer quantum scattering time in the δ-doped sample, attributed to the lowering of IR scattering, enabled by δ-doping. The experimental measurement of these fundamental transport properties is essential not only for designing heterostructures with improved electronic transport but also for enhancing the accuracy of device modeling. These insights hold significant technological and scientific value for advancing nitride-based electronic devices.

See the supplementary material for (1) R_{xx} measurements across the full magnetic field range, including a focus on the SdH oscillation onsets, (2) details on background resistance subtraction to obtain ΔR_{xx}, and (3) the procedure to deconvolve two oscillatory components in ΔR_{xx} of δ-doped sample.

The authors would like to thank Xiaoxi Huang and Anand Ithepalli for their assistance with wire bonding at Cornell University. This work was supported by the Army Research Office under Grant No. W911NF2220177 (characterization); ULTRA, an Energy Frontier Research Center funded by the U.S. Department of Energy (DOE), Office of Science, Basic Energy Sciences (BES), under Award No. DE-SC0021230 (modeling); and the DARPA THREADS program (epitaxial growth). This work made use of the Cornell Center for Materials Research shared instrumentation facility, which was supported through the NSF MRSEC program (DMR-1719875) and the Kavli Institute at Cornell (KIC).

AUTHOR DECLARATIONS

Conflict of Interest

The authors have no conflicts to disclose.

Author Contributions

Yu-Hsin Chen: Conceptualization (equal); Data curation (equal); Formal analysis (equal); Investigation (equal); Methodology (equal); Validation (equal); Writing – original draft (equal). **Jimy Encomendero:** Conceptualization (supporting); Formal analysis (supporting); Investigation (supporting); Validation (supporting); Writing – review & editing (supporting). **Chuan F. C. Chang:** Methodology (supporting). **Huili Grace Xing:** Funding acquisition (lead); Investigation (supporting); Project administration (lead); Resources (lead); Supervision (lead); Writing – review & editing (supporting). **Debdeep Jena:** Conceptualization (equal); Funding acquisition (equal); Investigation (equal); Project administration (equal); Resources (equal); Supervision (equal); Writing – review & editing (equal).

DATA AVAILABILITY

The data that support the findings of this study are available from the corresponding author upon reasonable request.

REFERENCES

[1]M. A. Khan, J. Kuznia, J. Van Hove, N. Pan, and J. Carter, "Observation of a two-dimensional electron gas in low pressure metalorganic chemical vapor deposited GaN-$Al_xGa_{1-x}N$ heterojunctions," Appl. Phys. Lett. **60**, 3027–3029 (1992).
[2]M. Asif Khan, A. Bhattarai, J. Kuznia, and D. Olson, "High electron mobility transistor based on a GaN-$Al_xGa_{1-x}N$ heterojunction," Appl. Phys. Lett. **63**, 1214–1215 (1993).
[3]U. K. Mishra, L. Shen, T. E. Kazior, and Y.-F. Wu, "GaN-based RF power devices and amplifiers," Proc. IEEE **96**, 287–305 (2008).
[4]U. K. Mishra, P. Parikh, and Y.-F. Wu, "AlGaN/GaN HEMTs-an overview of device operation and applications," Proc. IEEE **90**, 1022–1031 (2002).
[5]H. Amano, Y. Baines, E. Beam, M. Borga, T. Bouchet, P. R. Chalker, M. Charles, K. J. Chen, N. Chowdhury, R. Chu *et al.*, "The 2018 GaN power electronics roadmap," J. Phys. D **51**, 163001 (2018).
[6]T. J. Flack, B. N. Pushpakaran, and S. B. Bayne, "GaN technology for power electronic applications: A review," J. Electron. Mater. **45**, 2673–2682 (2016).
[7]M. Qi, G. Li, S. Ganguly, P. Zhao, X. Yan, J. Verma, B. Song, M. Zhu, K. Nomoto, H. G. Xing *et al.*, "Strained GaN quantum-well FETs on single crystal bulk AlN substrates," Appl. Phys. Lett. **110**, 063501 (2017).
[8]R. Chaudhuri, *Integrated Electronics on Aluminum Nitride: Materials and Devices* (Springer Nature, 2022).
[9]Y.-H. Chen, J. Encomendero, C. Savant, V. Protasenko, H. G. Xing, and D. Jena, "Electron mobility enhancement by electric field engineering of AlN/GaN/AlN quantum-well HEMTs on single-crystal AlN substrates," Appl. Phys. Lett. **124**, 152111 (2024).
[10]Y.-H. Chen, J. Encomendero, C. Savant, V. Protasenko, H. G. Xing, and D. Jena, "High conductivity coherently strained quantum well XHEMT heterostructures on AlN substrates with delta doping," Appl. Phys. Lett. **125**, 142110 (2024).
[11]R. T. Bondokov, S. P. Branagan, N. Ishigami, J. Grandusky, T. Nagatomi, K. Tatsuta, T. Miebach, and J. J. Chen, "Two-inch aluminum nitride (AIN) single crystal growth for commercial applications," ECS Trans. **104**, 37 (2021).
[12]T. Wang, J. Bai, S. Sakai, Y. Ohno, and H. Ohno, "Magnetotransport studies of AlGaN/GaN heterostructures grown on sapphire substrates: Effective mass and scattering time," Appl. Phys. Lett. **76**, 2737–2739 (2000).
[13]A. Kurakin, S. Vitusevich, S. Danylyuk, H. Hardtdegen, N. Klein, Z. Bougrioua, A. Naumov, and A. Belyaev, "Quantum confinement effect on the effective mass in two-dimensional electron gas of AlGaN/GaN heterostructures," J. Appl. Phys. **105**, 073703 (2009).
[14]T.-T. Wang, S. Dong, Z.-L. Xiao, C. Li, W.-C. Yue, B.-X. Liang, F.-F. Xu, Y.-L. Wang, S.-R. Xu, X.-L. Lu *et al.*, "Interface roughness governed negative magnetoresistances in two-dimensional electron gases in AlGaN/GaN heterostructures," Phys. Rev. Mater. **5**, 064003 (2021).
[15]L. Wong, S. Cai, R. Li, K. Wang, H. Jiang, and M. Chen, "Magnetotransport study on the two-dimensional electron gas in AlGaN/GaN heterostructures," Appl. Phys. Lett. **73**, 1391–1393 (1998).
[16]D. Hang, C.-T. Liang, C. Huang, Y. Chang, Y. Chen, H. Jiang, and J. Lin, "Effective mass of two-dimensional electron gas in an $Al_{0.2}Ga_{0.8}N$/GaN heterojunction," Appl. Phys. Lett. **79**, 66–68 (2001).
[17]A. Saxler, P. Debray, R. Perrin, S. Elhamri, W. Mitchel, C. Elsass, I. Smorchkova, B. Heying, E. Haus, P. Fini *et al.*, "Characterization of an AlGaN/GaN two-dimensional electron gas structure," J. Appl. Phys. **87**, 369–374 (2000).
[18]S. Elhamri, R. Newrock, D. Mast, M. Ahoujja, W. Mitchel, J. Redwing, M. Tischler, and J. Flynn, "$Al_{0.15}Ga_{0.85}N$/GaN heterostructures: Effective mass and scattering times," Phys. Rev. B **57**, 1374 (1998).
[19]L. Yang, X. Wang, T. Wang, J. Wang, W. Zhang, P. Quach, P. Wang, F. Liu, D. Li, L. Chen *et al.*, "Three subband occupation of the two-dimensional electron gas in ultrathin barrier AlN/GaN heterostructures," Adv. Funct. Mater. **30**, 2004450 (2020).
[20]J. Yaita, K. Fukuda, A. Yamada, T. Iwasaki, S. Nakaharai, and J. Kotani, "Improved channel electron mobility through electric field reduction in GaN quantum-well double-heterostructures," IEEE Electron Device Lett. **42**, 1592–1595 (2021).
[21]Z. Fan, J. Li, M. Nakarmi, J. Lin, and H. Jiang, "AlGaN/GaN/AlN quantum-well field-effect transistors with highly resistive AlN epilayers," Appl. Phys. Lett. **88**, 073513 (2006).
[22]R. Sladek, "Magnetoresistance oscillations in single-crystal and polycrystalline indium arsenide," Phys. Rev. **110**, 817 (1958).
[23]W. Zhang, C.-N. Kuo, S.-T. Kuo, C. W. So, J. Xie, K. T. Lai, W. C. Yu, C. S. Lue, H. C. Po, and S. K. Goh, "Tunable non-Lifshitz–Kosevich temperature dependence of Shubnikov–de Haas oscillation amplitudes in SmSb," npj Quantum Mater. **8**, 55 (2023).
[24]A. Okazaki, S. Wiedmann, S. Pezzini, M. Peres, P. Rappl, and E. Abramof, "Shubnikov–de Haas oscillations in topological crystalline insulator SnTe (111) epitaxial films," Phys. Rev. B **98**, 195136 (2018).
[25]R. Kubo, H. Hasegawa, and N. Hashitsume, "Quantum theory of galvanomagnetic effect I. Basic considerations," J. Phys. Soc. Jpn. **14**, 56–74 (1959).
[26]R. Dingle, "Some magnetic properties of metals II. The influence of collisions on the magnetic behaviour of large systems," Proc. R. Soc. London, Ser. A **211**, 517–525 (1952).
[27]T. Ihn, *Semiconductor Nanostructures: Quantum States and Electronic Transport* (OUP Oxford, 2009).
[28]D. Jena, *Quantum Physics of Semiconductor Materials and Devices* (Oxford University Press, 2022).
[29]C. Dreyer, A. Janotti, and C. Van de Walle, "Effects of strain on the electron effective mass in GaN and AlN," Appl. Phys. Lett. **102**, 142105 (2013).
[30]S. Syed, J. Heroux, Y. Wang, M. Manfra, R. Molnar, and H. Stormer, "Nonparabolicity of the conduction band of wurtzite GaN," Appl. Phys. Lett. **83**, 4553–4555 (2003).
[31]J. Harrang, R. Higgins, R. Goodall, P. Jay, M. Laviron, and P. Delescluse, "Quantum and classical mobility determination of the dominant scattering mechanism in the two-dimensional electron gas of an AlGaAs/GaAs heterojunction," Phys. Rev. B **32**, 8126 (1985).
[32]L. Hsu and W. Walukiewicz, "Transport-to-quantum lifetime ratios in AlGaN/GaN heterostructures," Appl. Phys. Lett. **80**, 2508–2510 (2002).